Research Square

Preprints are preliminary reports that have not undergone peer review.
They should not be considered conclusive, used to inform clinical practice,
or referenced by the media as validated information.

Green Microwave Combustion Synthesis of Magnesium Ferrite Nanoparticles Using Tinospora cordifolia for Electrical Relaxation Studies

Shivshankar Prasad Panday
Government E. R. R. Science P. G. College, Bilaspur, Chhattisgarh, India
K. P. Tiwari
Government E. R. R. Science P. G. College, Bilaspur, Chhattisgarh, India
H. S. Tewari
Guru Ghasidas Vishwavidyalaya
Abhishek Sharma
abhisheksharma@cvru.ac.in
Dr. C. V. Raman University
Vinayak Sahu
Swamai Atmanand Government English Medium College

Research Article

Keywords: MgFe2O4 Giloy, microwave-assisted green combustion, spinel ferrite, dielectric properties, electric modulus, electrical relaxation

Posted Date: November 19th, 2026

DOI: https://doi.org/10.21203/rs.3.rs-11239070/v1

License: This work is licensed under a Creative Commons Attribution 4.0 International License.
Read Full License

Additional Declarations: No competing interests reported.

Green Microwave Combustion Synthesis of Magnesium Ferrite Nanoparticles Using Tinospora cordifolia for Electrical Relaxation Studies

Shivshankar Prasad Pandey[1]*, K. P. Tiwari[1], H. S. Tewari[2], A. Sharma[3]* V.Sahu[4*]

[1] Government E. R. R. Science P. G. College, Bilaspur, Chhattisgarh, India

[2] Department of Pure and Applied Physics, Guru Ghasidas Vishwavidyalaya, Bilaspur, Chhattisgarh, India

[3] Department of Chemistry, Dr. C. V. Raman University, Kota, Bilaspur, Chhattisgarh, India

[4] Department of Chemistry, Swamai Atmanand Government English Medium College, Raipur, Chhattisgarh, India

*** Corresponding author: abhisheksharma@cvru.ac.in, vinayaksahu2208@gmail.com , shivpandeybsp@gmail.com**

Abstract

Nanocrystalline $MgFe_2O_4$ was synthesized through a rapid microwave-assisted green combustion route using Tinospora cordifolia (Giloy) stem extract as a naturally derived fuel and complexing medium. The combustion process produced crystalline $MgFe_2O_4$directly without requiring post-synthesis calcination, demonstrating the effectiveness of plant-derived phytochemicals in promoting spinel ferrite formation. X-ray diffraction confirmed a single-phase cubic spinel structure (space group $Fd\bar{3}m$), while crystallite sizes determined using the Debye-Scherrer, Williamson-Hall (W-H), and Size-Strain Plot (SSP) methods were 15.10, 18.36, and 18.26 nm, respectively, indicating good crystallinity with only minor lattice strain. FTIR spectra exhibited the characteristic metal-oxygen vibrations of the spinel lattice, whereas SEM revealed a porous agglomerated morphology produced during rapid combustion. EDS analysis verified Mg, Fe, and O as the principal constituent elements without detectable metallic impurities. Frequency- and temperature-dependent electrical measurements (1 Hz–100 kHz, room temperature to 400 °C) showed pronounced dielectric dispersion together with thermally enhanced dielectric permittivity, loss, and AC conductivity. Electric modulus analysis revealed a broad distribution of relaxation times, confirming non-Debye relaxation behaviour. Arrhenius analysis of the selected high-temperature M″ relaxation branch yielded an activation energy of 0.758 eV, indicating thermally activated electron hopping between Fe^{2+} and Fe^{3+} ions. The results demonstrate that the Giloy-assisted microwave combustion approach provides an efficient and environmentally sustainable route for producing nano crystalline $MgFe_2O_4$ with favourable dielectric characteristics suitable for frequency-dependent ferrite applications.

Keywords: $MgFe_2O_4$ Giloy; microwave-assisted green combustion; spinel ferrite; dielectric properties; electric modulus; electrical relaxation

1. Introduction

Spinel ferrites, represented by the general formula $MgFe_2O_4$ (*M* = divalent metal ion), constitute an important class of magnetic oxide materials because of their structural stability and versatile physical properties. Their electrical, magnetic, catalytic, and

dielectric characteristics can be tailored through appropriate selection of the divalent cation and synthesis conditions, making them attractive for applications such as high-frequency transformers, microwave absorbers, electromagnetic interference shielding, sensors, catalysts, lithium-ion batteries, and biomedical devices [6, 11, 18]. Among the various spinel ferrites, magnesium ferrite $MgFe_2O_4$ has received considerable attention owing to its relatively high electrical resistivity, low eddy-current loss, good chemical stability, moderate magnetic behaviour, and environmentally benign composition. These characteristics make $MgFe_2O_4$a promising candidate for dielectric and frequency-dependent electronic applications [7, 17, 24].

The performance of $MgFe_2O_4$is closely related to its crystal structure, crystallite size, cation distribution, and microstructure, all of which are governed by the synthesis route. Conventional preparation methods, including solid-state reaction, co-precipitation, hydrothermal synthesis, sol-gel processing, and combustion synthesis, have been widely employed to produce $MgFe_2O_4$nanoparticles. Although these techniques are capable of yielding phase-pure ferrites, they often involve prolonged heating, repeated grinding, or high-temperature calcination, increasing both processing time and energy consumption. Such conditions may also promote excessive particle growth and agglomeration, which can adversely influence the functional properties of the material [19, 21, 25]. Consequently, there is continued interest in developing rapid and energy-efficient synthesis methods that can produce highly crystalline $MgFe_2O_4$while minimizing processing complexity.

Green synthesis has emerged as a practical alternative by replacing conventional organic fuels with naturally derived materials rich in bioactive compounds. Plant extracts contain polyphenols, flavonoids, sugars, organic acids, and other phytochemicals capable of chelating metal ions and promoting combustion during oxide formation. Besides reducing the consumption of hazardous chemicals, these naturally occurring compounds facilitate homogeneous mixing of precursor ions and can influence nucleation, crystal growth, and particle morphology. As a result, plant-mediated synthesis has become an increasingly attractive approach for preparing ferrite nanomaterials using environmentally sustainable processing routes [3, 18].

Among medicinal plants, Giloy is particularly interesting because its stem extract contains abundant phenolic compounds, flavonoids, terpenoids, alkaloids, and polysaccharides that readily participate in complexation and combustion reactions. During microwave irradiation, these phytochemicals promote rapid decomposition of the precursor solution and assist in the formation of crystalline oxide nanoparticles. While Giloy has been extensively investigated for its medicinal and pharmacological properties, comparatively few studies have explored its application as a green combustion medium for synthesizing $MgFe_2O_4$nanoparticles or examined how the resulting microstructure influences dielectric relaxation and electrical conduction.

In the present work, nano crystalline $MgFe_2O_4$ was synthesized through a microwave-assisted green combustion method employing Giloy stem extract as the natural fuel and complexing agent. The structural characteristics of the synthesized material were investigated using X-ray diffraction (XRD), Fourier transform infrared spectroscopy (FTIR), scanning electron microscopy (SEM), and energy-dispersive X-ray spectroscopy (EDS). Its electrical behaviour was subsequently evaluated through frequency- and temperature-dependent dielectric measurements, AC conductivity, electric modulus analysis, and Arrhenius modelling. By establishing correlations

between the synthesis route, crystal structure, microstructure, and electrical response, this study demonstrates the potential of a plant-assisted microwave combustion strategy for producing $MgFe_2O_4$ nanoparticles suitable for advanced dielectric applications.

2. Experimental

2.1 Materials

Analytical-grade magnesium nitrate hexahydrate [$Mg(NO_3)_2 \cdot 6H_2O$] and ferric nitrate nonahydrate [$Fe(NO3)_3 \cdot 9H_2O$] were procured from commercial suppliers and used as received without further purification. Fresh stems of Giloy were collected by cutting stems from a plant growing in the author's own garden at Usha Upavan Residential Colony, Lokhandi, Bilaspur, Chhattisgarh, India, and served as the natural source of phytochemicals for the green combustion process. Deionized water was used throughout the preparation of the plant extract and precursor solution.

2.2 Preparation of Giloy Extract

Fresh Giloy stems were thoroughly washed with tap water followed by deionized water to remove dust and other surface impurities. The cleaned stems were shade-dried and ground into a fine powder. Approximately 10 g of the powdered material was dispersed in 100 mL of deionized water and stirred at 600 rpm while maintaining the temperature at 60 °C for 40 min to facilitate the extraction of bioactive phytochemicals. After cooling to room temperature, the suspension was filtered through Whatman No. 1 filter paper, and the filtrate was stored at 4 °C until further use.

2.3 Synthesis of $MgFe_2O_4$ Nanoparticles

Stoichiometric quantities of magnesium nitrate hexahydrate and ferric nitrate nonahydrate corresponding to the composition $MgFe_2O_4$ were dissolved in the prepared Giloy extract under continuous magnetic stirring to obtain a homogeneous precursor solution. The phytochemicals present in the extract served as natural complexing agents and combustion promoters, ensuring uniform distribution of the metal ions throughout the solution.

The precursor solution was transferred to a borosilicate reaction vessel and irradiated in a domestic microwave oven operating at 2.45 GHz with an output power of 600 W. Within approximately 5 min, rapid dehydration was followed by spontaneous combustion, producing a voluminous porous mass accompanied by the evolution of gaseous reaction products. The as-combusted product was gently ground using an agate mortar and pestle to obtain a fine powder for subsequent characterization. No additional calcination step was employed, thereby preserving the simplicity and energy-efficient nature of the green synthesis route.

2.4 Characterization

The phase composition and crystal structure of the synthesized $MgFe_2O_4$ nanoparticles were examined by XRD using Cu Kα radiation (λ = 1.5406 Å). Diffraction data were analyzed using the Debye-Scherrer, W–H, and SSP methods to evaluate the crystallite size and lattice strain.

The chemical bonding and vibrational characteristics were investigated by FTIR over the spectral range of 4000–400 cm^{-1}. Surface morphology was examined using SEM,

while the elemental composition was determined by EDS attached to the SEM system.

For electrical measurements, the synthesized $MgFe_2O_4$ nanopowder was compacted into circular pellets of approximately 13 mm diameter and 1.28 mm thickness using a hydraulic press. Both pellet surfaces were coated with conductive silver paste to ensure good electrical contact. Frequency- and temperature-dependent dielectric measurements were carried out over the range of 1 Hz–100 kHz from room temperature to 400 °C. The dielectric constant (ε′), dielectric loss (ε″), loss tangent (tan δ), AC conductivity (σ_{ac}), and electric modulus (M′ and M″) were calculated using the following expressions:

$$\varepsilon' = \frac{c_P \mathrm{t}}{\varepsilon_0 \mathrm{A}}$$

$$\varepsilon'' = \varepsilon' \tan\delta$$

$$\sigma_{ac} = 2\pi \mathrm{f} \varepsilon_0 \varepsilon''$$

$$M' = \frac{\varepsilon'}{\varepsilon'^2 + \varepsilon''^2}$$

$$M'' = \frac{\varepsilon''}{\varepsilon'^2 + \varepsilon''^2}$$

where C_p is the measured capacitance, t is the pellet thickness, A is the electrode area, ε_0 is the permittivity of free space, and f is frequency.

The relaxation time corresponding to the selected M″ relaxation features was determined using

$$\tau = \frac{1}{2\pi \mathrm{f}_{\max}}$$

and the activation energy was obtained from the Arrhenius equation,

$$\tau = \tau_0 \exp \frac{\mathrm{E_a}}{\mathrm{k_B T}}$$

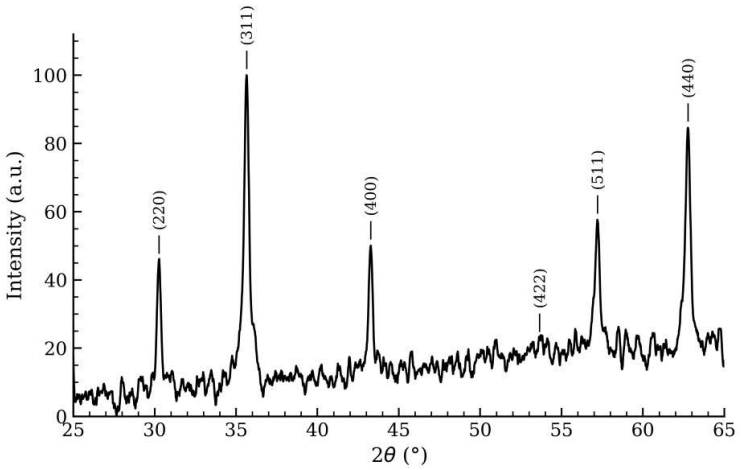
where τ_0 is the pre-exponential factor, E_a is the activation energy, k_B is Boltzmann's constant, and T is the absolute temperature. Bulk density was calculated from pellet mass and geometry; apparent porosity was obtained by comparison with the X-ray density.

3. Results and Discussion

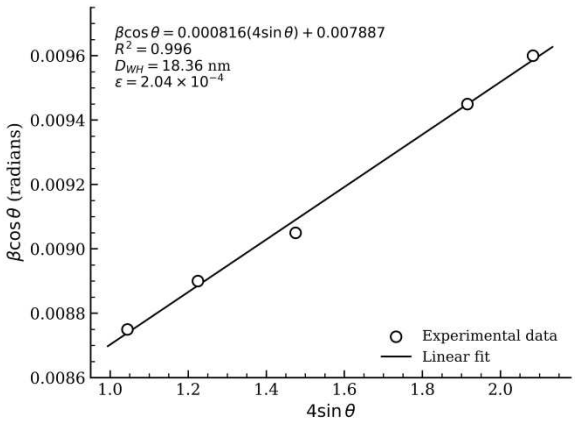
3.1 Structural Characterization by XRD

The XRD pattern of the $MgFe_2O_4$ nanoparticles synthesized through the microwave-assisted Giloy-assisted green combustion process is presented in Fig. 1. The diffraction profile consists exclusively of reflections characteristic of cubic spinel $MgFe_2O_4$, indicating that the selected synthesis route promotes direct formation of the ferrite phase within a short reaction period. All diffraction maxima can be indexed to the (220), (311), (400), ($\bar{5}$11), and (440) crystallographic planes of the cubic spinel structure (space group $Fd\bar{3}m$), in good agreement with the corresponding standard diffraction data (ICDD PDF No. 88-1935). No additional reflections associated with magnesium oxide, hematite, or other crystalline impurity phases are observed, confirming the high phase purity of the synthesized material [12, 17, 24].

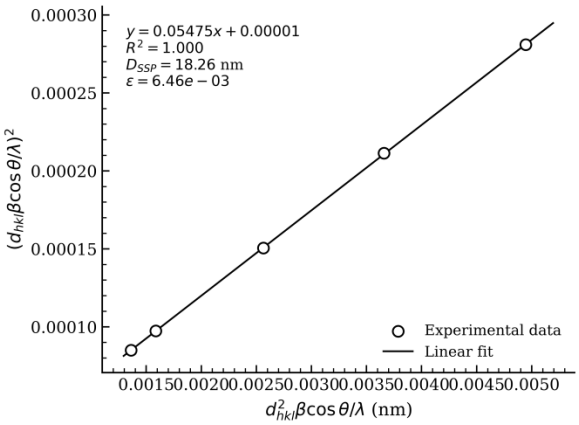
The absence of secondary phases demonstrates that the phytochemical constituents of the Giloy extract effectively assisted precursor complexation and combustion during microwave irradiation. Rapid volumetric heating under microwave energy accelerates precursor decomposition and facilitates simultaneous nucleation throughout the reaction medium, thereby promoting crystallization of the spinel phase without the prolonged thermal treatment generally required by conventional ceramic processing. This observation highlights the effectiveness of combining microwave heating with a plant-derived combustion medium to obtain crystalline $MgFe_2O_4$ through an energy-efficient synthesis route [18, 25].



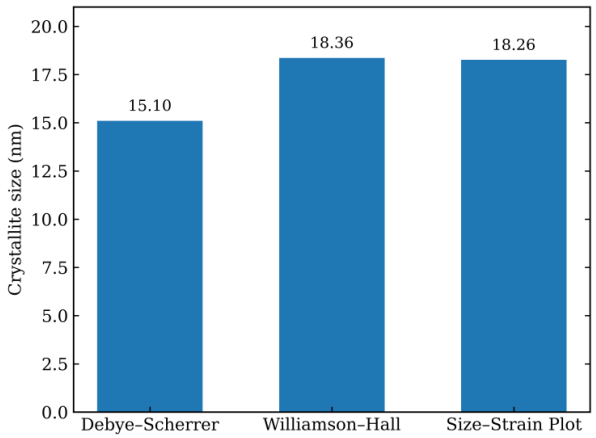
(a)



(b)



(c)



(d)

Fig. 1 X-ray diffraction pattern of $MgFe_2O_4$ nanoparticles (a), W–H plot (b), SSP analysis (c), and comparison of crystallite sizes estimated by the Debye–Scherrer, W–H, and SSP methods (d)

Although the combustion reaction was completed within a few minutes, the diffraction peaks remain sharp and well resolved, indicating good crystallinity. At the same time, measurable peak broadening confirms that the coherent diffraction domains remain within the nanometre range. Such behaviour is typical of microwave-derived ferrite nanoparticles, where rapid nucleation restricts excessive grain growth while maintaining satisfactory crystal ordering.

To obtain a reliable estimate of the crystallite dimensions, the diffraction data were analysed using three independent approaches: the Debye-Scherrer equation, the W-H method, and the SSP model. The average crystallite sizes obtained from these methods were 15.10 nm, 18.36 nm, and 18.26 nm, respectively. The close agreement among the three calculations indicates that crystallite-size broadening represents the dominant contribution to the observed peak widths, whereas lattice strain contributes only to a limited extent. The slightly higher values predicted by the W–H and SSP analyses arise because these methods account for strain-induced broadening in addition to the finite crystallite size, providing a more comprehensive description of the diffraction profile than the Debye-Scherrer approximation alone[4, 6].

Further analysis of the diffraction data yielded lattice parameters consistent with those reported for stoichiometric cubic $MgFe_2O_4$ The corresponding unit-cell volume, X-ray density, bulk density, and porosity likewise fall within the range commonly reported for combustion-derived magnesium ferrites. The moderate porosity is attributed to the rapid evolution of gaseous products during microwave combustion, which prevents complete particle densification and generates interconnected pores throughout the powder. This porous architecture is expected to influence the electrical response by increasing the number of grain-boundary interfaces available for charge accumulation under an alternating electric field, an aspect discussed in the subsequent dielectric analysis [3, 20].

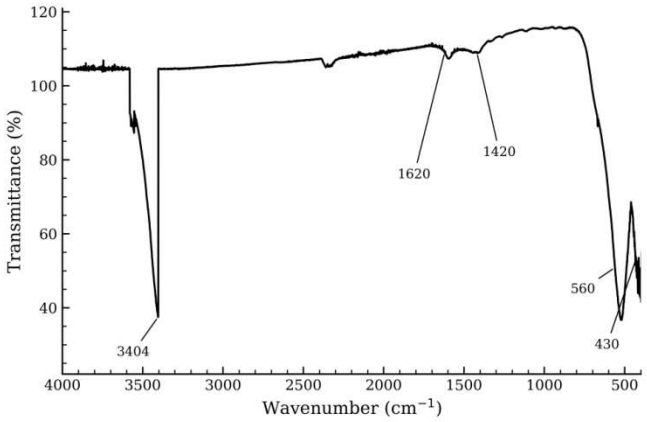
The diffraction analysis demonstrates that the microwave-assisted Giloy combustion route produces phase-pure nanocrystalline $MgFe_2O_4$ with good crystallinity and minimal residual lattice strain. The structural characteristics established by XRD provide the foundation for interpreting the vibrational, microstructural, and electrical behaviour presented in the following sections.

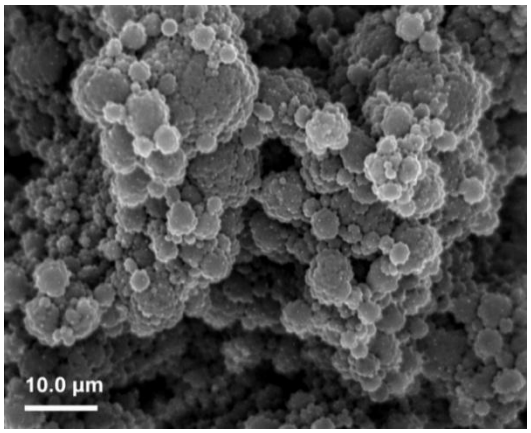
3.2 FTIR, SEM and EDS Analysis

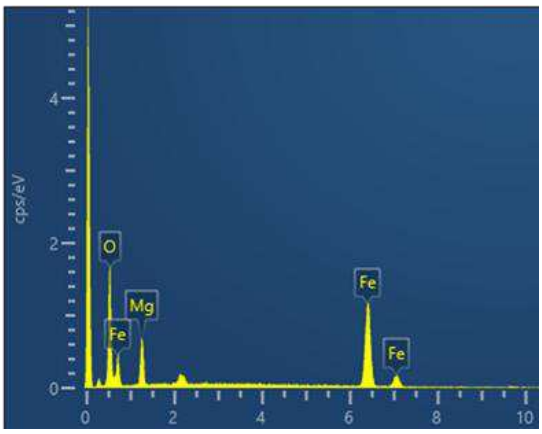
The structural information obtained from XRD was further examined through FTIR,SEM, and EDS. While XRD establishes the long-range crystal structure, these complementary techniques provide insight into local bonding, combustion-derived morphology, and elemental composition, allowing a more comprehensive understanding of the synthesized $MgFe_2O_4$ nanoparticles.

The FTIR spectrum shown in Fig. 2(a) exhibits the characteristic vibrational features of the spinel ferrite lattice. Two well-defined absorption bands located at approximately 560 cm^{-1} and 430 cm^{-1} are assigned to the stretching vibrations of metal-oxygen bonds associated predominantly with the tetrahedral (A) and

octahedral (B) coordination sites, respectively. The presence of these bands confirms the formation of the spinel framework identified by XRD. Their positions are consistent with previously reported $MgFe_2O_4$ nanoparticles synthesized by combustion, sol-gel, and other wet-chemical methods [15, 17, 24].







Spectrum 1				
Element	**Line Type**	**Weight %**	**Weight % Sigma**	**Atomic %**
O	K series	20.61	0.44	44.01
Mg	K series	9.35	0.31	13.14
Fe	K series	70.04	0.53	42.85
Total		100		100

Fig. 2 FTIR spectrum showing the characteristic metal–oxygen vibrations of $MgFe_2O_4$ (a), SEM micrograph illustrating the irregular porous and agglomerated powder morphology (b), and EDS spectrum with corresponding elemental composition (c)

Besides the characteristic lattice vibrations, a broad absorption centred near 3404 cm^{-1} together with a weaker feature around 1620 cm^{-1} is attributed to stretching and bending vibrations of adsorbed water molecules and surface hydroxyl groups. A low-intensity band near 1420 cm^{-1} is associated with trace carbonate species formed through atmospheric CO_2 adsorption during cooling and storage of the powder. The relatively weak intensity of these absorptions, combined with the absence of corresponding impurity reflections in the XRD pattern, indicates that they originate from surface adsorption rather than residual precursor compounds or secondary crystalline phases.

The SEM micrograph presented in Fig. 2(b) reveals an interconnected porous microstructure composed of irregular secondary agglomerates. Such morphology is characteristic of microwave-assisted combustion synthesis, where rapid decomposition of nitrate precursors and oxidation of plant-derived organic constituents generate a large volume of gaseous products within a short time. The escaping gases inhibit complete particle densification and produce numerous interconnected pores throughout the agglomerated powder. Although the primary

nanocrystallites cannot be individually resolved at the selected magnification, the observed agglomerates are assembled from much finer crystalline domains, in agreement with the nanometre-scale crystallite sizes determined from XRD. Similar porous combustion-derived morphologies have been reported for $MgFe_2O_4$ synthesized using environmentally benign combustion routes [5, 14, 23].

The porous architecture observed by SEM is expected to influence the electrical behaviour of the compacted pellets. Grain boundaries surrounding these agglomerates act as electrically resistive regions where charge carriers accumulate under an alternating electric field, thereby contributing to interfacial polarization and dielectric relaxation. Consequently, the microstructural characteristics identified here provide an important physical basis for interpreting the dielectric and electrical properties discussed in the subsequent sections.

The EDS spectrum together with the quantitative elemental analysis is presented in Fig. 2(c). Magnesium, iron, and oxygen are identified as the principal constituent elements of the synthesized powder, confirming successful incorporation of the precursor ions into the ferrite structure. No additional metallic impurities are detected within the instrumental detection limit, demonstrating the chemical purity of the synthesized $MgFe_2O_4$ The measured elemental percentages differ slightly from the ideal stoichiometric composition, particularly for oxygen, which is expected because EDS provides localized semi-quantitative analysis and has limited sensitivity for light elements. Variations associated with surface roughness, interaction volume, and the selected analysis area may also contribute to these deviations. Therefore, the EDS results should be interpreted as confirmation of elemental composition rather than precise determination of bulk stoichiometry.

Taken together, the FTIR, SEM, and EDS results complement the XRD analysis by confirming the successful formation of nanocrystalline $MgFe_2O_4$ through the Giloy-assisted microwave combustion route. The combination of a well-developed spinel framework, porous combustion-derived microstructure, and chemically pure Mg–Fe–O composition establishes a consistent structural basis for the dielectric and electrical behaviour discussed in the following sections.

3.3 Frequency- and Temperature-Dependent Dielectric Properties

The dielectric response of the microwave-synthesized $MgFe_2O_4$ nanoparticles was evaluated over the frequency range of 1 Hz–100 kHz at temperatures extending from room temperature to 400 °C. Representative ε′ and ε″ curves recorded at selected frequencies are presented in Fig. 3(a,b). The measurements demonstrate that both frequency and temperature strongly influence the electrical polarization of the synthesized ferrite.

A pronounced dielectric dispersion is observed throughout the investigated temperature range. The largest values of ε′ occur at lower frequencies, whereas the dielectric constant progressively decreases as the measurement frequency increases. This behaviour indicates that the various polarization processes present in the material respond differently to the applied alternating electric field. During low-frequency measurements, the electric field changes sufficiently slowly to permit localized charge carriers to migrate over comparatively long distances and accumulate at internal interfaces, thereby producing a large dielectric response. As the field oscillates more rapidly, these slower polarization processes become increasingly unable to follow the field reversal, leading to the gradual reduction in

dielectric permittivity observed at higher frequencies. Influence of temperature is equally evident. Raising the measurement temperature produces a systematic increase in ε′ at all investigated frequencies, although the magnitude of the increase is considerably greater at the lower frequencies. The additional thermal energy enhances the mobility of localized charge carriers within the ferrite lattice, allowing a larger fraction of the available polarization mechanisms to participate in the dielectric response. Consequently, the material exhibits progressively stronger polarization as the temperature increases. Similar temperature-dependent behaviour has been reported for nanocrystalline magnesium ferrites prepared by combustion and solution-based synthesis routes, where thermally activated carrier motion governs the dielectric response [10, 13, 22].

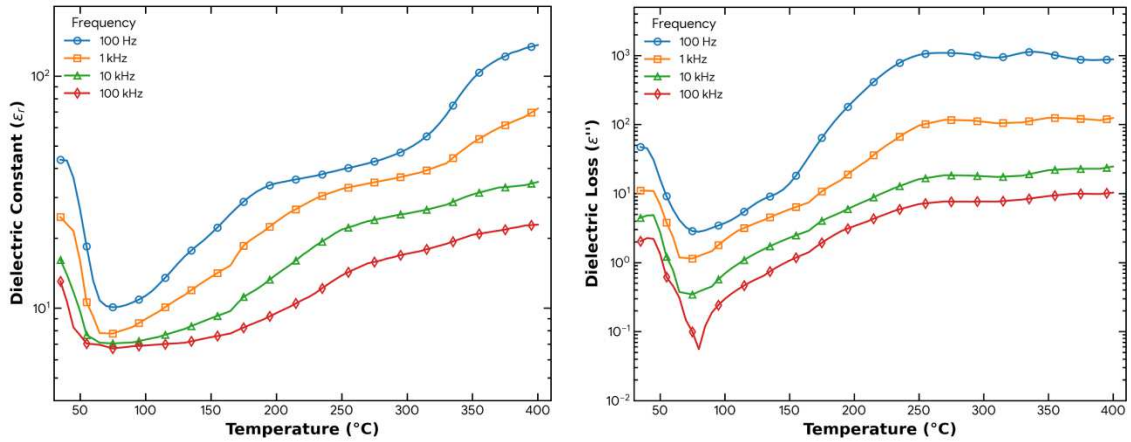


Fig. 3 Temperature dependence of ε' (a) and ε" (b) of as-synthesized $MgFe_2O_4$ nanoparticles measured at 100 Hz, 1 kHz, 10 kHz, and 100 kHz

Electrical behaviour observed in the present study is closely associated with the combustion-derived microstructure identified by SEM. Rapid gas evolution during microwave combustion generates a porous network composed of relatively conducting grains separated by more resistive grain-boundary regions. These heterogeneous microstructural features create numerous interfaces capable of trapping mobile charge carriers under an alternating electric field. At lower frequencies, sufficient time is available for charge accumulation at these interfaces, resulting in enhanced interfacial polarization. Increasing the measurement frequency progressively suppresses this contribution because charge carriers can no longer respond completely within each field cycle. The measured dielectric dispersion therefore reflects the combined influence of the nanocrystalline spinel structure and the porous grain-boundary network produced during the green combustion process rather than a single polarization mechanism.

The Variation of ε″, illustrated in Fig. 3(b), follows a trend comparable to that observed for ε′. ε″ increases gradually with temperature while remaining considerably larger at lower frequencies than at higher frequencies. This behaviour indicates that energy dissipation becomes more pronounced as thermally activated charge carriers acquire sufficient mobility to participate in polarization and short-range hopping processes. In contrast, the comparatively small ε″ values recorded at 100 kHz demonstrate that slower relaxation processes contribute only minimally under rapidly alternating electric fields. The absence of abrupt anomalies in either ε′ or ε″ further suggests that the dielectric response evolves continuously throughout the

investigated temperature range, supporting the existence of distributed rather than discrete relaxation processes [7, 17].

Overall, the dielectric measurements establish that the microwave-assisted Giloy combustion route produces $MgFe_2O_4$ nanoparticles exhibiting stable frequency-dependent dielectric behaviour together with thermally activated polarization. The close correspondence between the dielectric response and the microstructural characteristics identified by XRD and SEM demonstrates that both crystallographic and microstructural features contribute to the observed electrical behaviour.

3.4 Electrical Conduction Behaviour

The Mechanisms responsible for dielectric polarization can be understood more clearly by examining the tan δ and σ_{ac}, which are presented in Fig. 4(a,b). These parameters provide complementary information on energy dissipation and charge transport during the application of an alternating electric field and therefore assist in identifying the dominant conduction process operating in the synthesized $MgFe_2O_4$ nanoparticles.

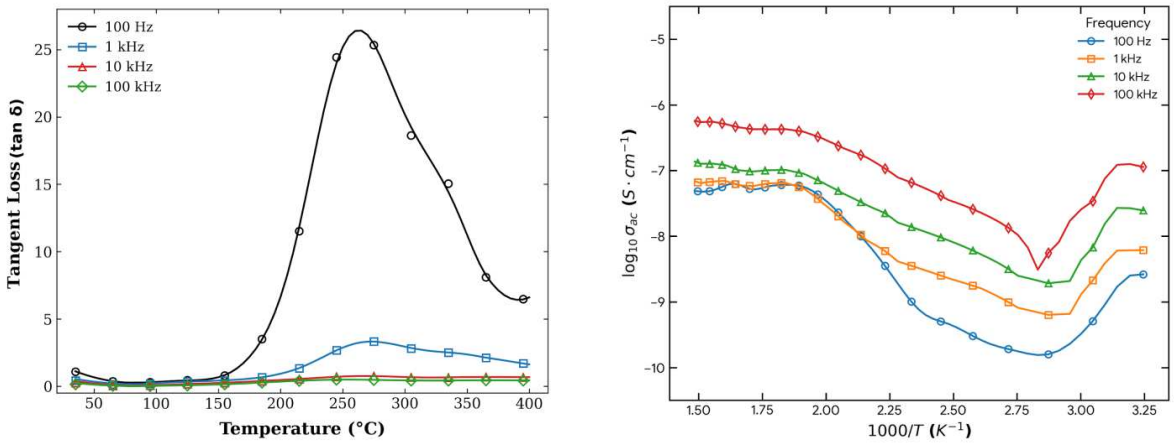


Fig. 4 Temperature-dependent electrical properties of $MgFe_2O_4$ nanoparticles: tan δ (a) and $\log_{10}\sigma_{ac}$ versus 1000/T (b) at representative frequencies

The temperature dependence of the dielectric loss tangent is shown in Fig. 4(a). At lower temperatures, tan δ remains comparatively small throughout the investigated frequency range, indicating limited dielectric energy dissipation. As the temperature increases, however, the loss gradually becomes more pronounced, particularly at the lower frequencies. This behaviour reflects the increasing participation of thermally activated charge carriers in the polarization process. Additional thermal energy enhances the mobility of localized electrons, enabling them to respond more effectively to the alternating electric field and thereby increasing dielectric relaxation.

A noticeable reduction in tan δ is observed with increasing frequency. Under rapidly oscillating electric fields, slowly responding polarization processes no longer contribute significantly to the dielectric response because the available time during each cycle becomes insufficient for complete charge redistribution. Consequently, dielectric loss decreases progressively at higher frequencies, where the electrical response is governed primarily by faster polarization mechanisms. The comparatively low dielectric loss maintained in this frequency region is advantageous for dielectric materials intended for high-frequency operation because it minimizes energy dissipation during repeated electrical cycling [2, 8, 17].

The temperature dependence of AC conductivity is illustrated in Fig. 4(b). In contrast to the dielectric constant, electrical conductivity increases continuously with temperature at all investigated frequencies. This behaviour demonstrates that charge transport in the synthesized $MgFe_2O_4$ is a thermally activated process. Increasing temperature provides sufficient energy for localized electrons to overcome potential barriers separating neighbouring iron ions, thereby increasing the probability of electron exchange between Fe^{2+} and Fe^{3+} ions located at octahedral sites within the spinel lattice. The progressive increase in conductivity therefore reflects enhanced hopping conduction rather than the generation of free electronic carriers.The influence of frequency is equally important. At higher frequencies, repeated field oscillations increase the probability of localized hopping events within the conducting grains, resulting in a gradual increase in AC conductivity. The nanocrystalline microstructure produced during microwave combustion also contributes to this behaviour. Conductive grain interiors are separated by comparatively resistive grain boundaries, producing a heterogeneous electrical network in which the relative contribution of grains becomes increasingly dominant as the measurement frequency increases. This interpretation is fully consistent with the porous morphology observed by SEM and the dielectric dispersion discussed in the previous section [1, 7, 22].

The combined behaviour of tan δ and σ_{ac} demonstrates that dielectric relaxation and electrical conduction originate from the same thermally activated hopping mechanism. Rather than acting as independent processes, polarization and charge transport evolve simultaneously with increasing temperature, both being governed by localized electron motion within the spinel framework. The agreement between the dielectric, conductivity, and structural observations therefore provides strong evidence that the electrical response of the present $MgFe_2O_4$ nanoparticles is controlled predominantly by short-range hopping between mixed-valence iron ions**.**

3.5 Electric Modulus Analysis and Electrical Relaxation

While dielectric permittivity emphasizes polarization processes, the electric modulus formalism provides a clearer description of the intrinsic relaxation dynamics by minimizing the influence of electrode polarization and interfacial charge accumulation. Consequently, the M′ and M″ components of the electric modulus were analysed to obtain further insight into the relaxation behaviour of the synthesized $MgFe_2O_4$ nanoparticles. The corresponding results are presented in Fig. 5(a,b).

The variation of the M′ with temperature is shown in Fig. 5(a). At lower temperatures, M′ remains close to zero over the entire frequency range, indicating that long-range motion of charge carriers is highly restricted. Under these conditions, localized electrons remain confined within potential wells associated with the nanocrystalline lattice and grain-boundary regions, producing only a limited modulus response. As the temperature increases, M′ gradually rises, particularly at higher frequencies, reflecting the progressive activation of localized carriers. This continuous increase suggests that thermal energy enhances short-range hopping processes without producing an abrupt transition in the electrical response.

Behaviour of the M″, presented in Fig. 5(b), provides direct evidence of dielectric relaxation. Broad relaxation maxima are observed, and their positions shift systematically towards higher temperatures as the measuring frequency increases. This shift demonstrates that the characteristic relaxation time decreases with increasing temperature, indicating progressively faster charge-carrier dynamics.

Rather than exhibiting a single, sharply defined relaxation process, the broad nature of the M″ peaks reveals a distribution of relaxation times arising from the structural heterogeneity of the nanocrystalline material. Contributions from grain interiors, grain boundaries, and localized defect sites therefore occur simultaneously, resulting in non-Debye relaxation behaviour [17].

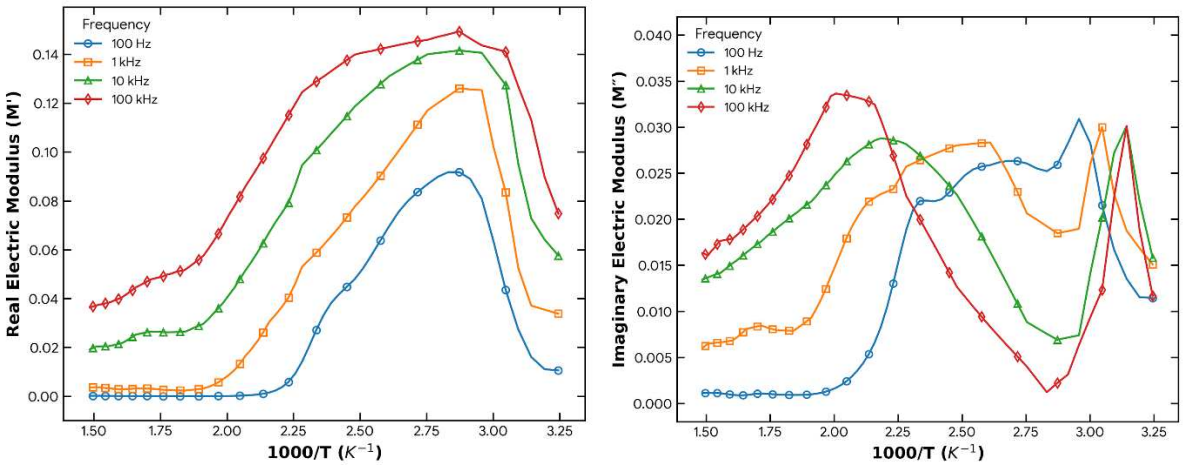


Fig. 5 Temperature dependence of M' (a) and M" (b) of $MgFe_2O_4$ nanoparticles measured at 100 Hz, 1 kHz, 10 kHz, and 100 kHz

The relaxation behaviour identified through the modulus formalism is closely associated with localized electron hopping between neighbouring Fe^{2+} and Fe^{3+} ions occupying octahedral sites within the spinel lattice. At relatively low temperatures, insufficient thermal energy limits the hopping probability, leading to comparatively slow relaxation. Increasing the temperature enhances carrier mobility, thereby shortening the relaxation time and shifting the M″ maxima towards higher temperatures. The porous microstructure produced during microwave-assisted combustion further broadens the relaxation spectrum by introducing grain-boundary regions with different local electrical environments. Consequently, relaxation occurs over a range of characteristic times rather than through a single uniform process.

Modulus analysis complements the dielectric and conductivity results discussed in the preceding sections. Whereas dielectric measurements describe the ability of the material to store electrical energy and conductivity measurements quantify charge transport, the modulus representation highlights the dynamic response of localized carriers responsible for dielectric relaxation. The excellent agreement among these independent electrical measurements confirms that the electrical behaviour of the synthesized $MgFe_2O_4$ nanoparticles is governed predominantly by thermally activated localized hopping within the spinel framework.

3.6 Arrhenius Analysis of Relaxation Process

The relaxation process identified from the electric modulus spectra was further evaluated using Arrhenius analysis. The relaxation time corresponding to each M″ maximum was calculated from

$$\tau = \frac{1}{2\pi f_{max}}$$

where f_{max} represents the frequency associated with the maximum value of the imaginary modulus. The temperature dependence of the relaxation time follows the Arrhenius relationship

$$\tau = \tau_0 exp\left(\frac{E_a}{k_B T}\right)$$

where τ_0 is the pre-exponential factor, E_a is the activation energy, k_B is the Boltzmann constant, and T is the absolute temperature.

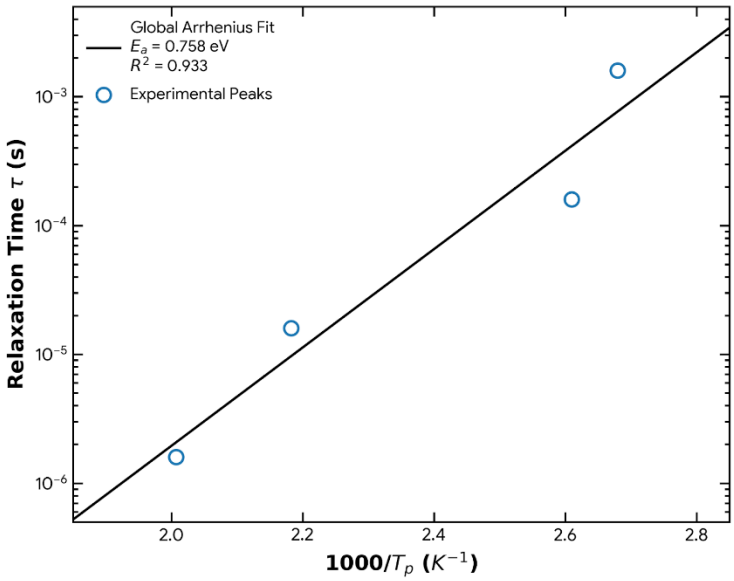


Fig. 6 Arrhenius plot of relaxation time obtained from the selected higher-temperature relaxation features of the M" spectra of $MgFe_2O_4$ nanoparticles; the solid line represents the linear fit

The Arrhenius plot shown in Fig. 6 exhibits an approximately linear relationship between ln(τ) and 1000/T, confirming that the relaxation process is thermally activated. Linear fitting of the experimental data yields an activation energy of 0.758 eV, which is characteristic of localized electron hopping between Fe^{2+} and Fe^{3+} ions occupying neighbouring octahedral sites in the spinel lattice. The magnitude of the activation energy is comparable to values reported for $MgFe_2O_4$ and related ferrite systems in which short-range hopping dominates electrical relaxation [9, 16, 22].

The activation energy obtained from the modulus analysis is consistent with the dielectric and conductivity measurements presented earlier. The increase in dielectric permittivity with temperature, the enhancement of AC conductivity, and the systematic displacement of the M″ relaxation maxima all arise from the same thermally activated hopping process. These observations collectively demonstrate that the electrical response of the present $MgFe_2O_4$ nanoparticles is governed by localized carrier dynamics rather than long-range band conduction, confirming the semiconducting nature of the material.

4. Conclusions

Nanocrystalline $MgFe_2O_4$ was successfully synthesized using a rapid microwave-assisted green combustion route in which Giloy stem extract served as a naturally derived complexing and combustion medium. The synthesis was completed within a

few minutes without any post-combustion calcination, demonstrating that plant-derived phytochemicals can effectively facilitate the formation of crystalline spinel ferrites through an energy-efficient and environmentally benign process.

Structural characterization confirmed the formation of a single-phase cubic spinel $MgFe_2O_4$ with good crystallinity and nanometre-sized crystallites. The crystallite sizes obtained from the Debye-Scherrer, W-H, and SSP analyses were in close agreement, indicating that crystallite-size broadening dominates the diffraction profile while residual lattice strain remains comparatively small. FTIR analysis verified the characteristic metal-oxygen vibrations associated with tetrahedral and octahedral lattice sites, whereas SEM revealed a porous agglomerated morphology produced by rapid gas evolution during microwave combustion. EDS further confirmed the presence of Mg, Fe, and O as the principal constituent elements without detectable metallic impurities.

Electrical measurements demonstrated that the dielectric response depends strongly on both frequency and temperature. The decrease in dielectric permittivity with increasing frequency and its enhancement at elevated temperatures indicate thermally activated polarization within the nanocrystalline spinel framework. The corresponding increase in σ_{ac}, together with the electric modulus behaviour, confirms that localized electron hopping between Fe^{2+} and Fe^{3+} ions is the dominant charge-transport mechanism. Broad relaxation peaks observed in the M″ spectra indicate a distribution of relaxation times characteristic of non-Debye behaviour. Arrhenius analysis yielded an activation energy of 0.758 eV, supporting the interpretation that dielectric relaxation is governed primarily by thermally activated hopping processes.

The combined structural and electrical results demonstrate that microwave-assisted Giloy-mediated green combustion is an effective strategy for producing phase-pure $MgFe_2O_4$ nanoparticles with stable dielectric behaviour and favourable electrical relaxation characteristics. The simplicity of the synthesis route, together with the use of a renewable plant-derived combustion medium, highlights its potential as a sustainable alternative for preparing ferrite nanomaterials intended for frequency-dependent dielectric and electronic applications. Further investigations involving magnetic characterization and device-level evaluation would provide additional insight into the wider application potential of these materials.

Funding

No funding was received for this research.

Data availability

The datasets generated and/or analysed during the current study are available from the corresponding author on reasonable request.

Ethics and consent to participate

The Tinospora cordifolia (Giloy) stem material used in this study was collected by cutting stems from a plant growing in the author's own garden at Usha Upavan Residential Colony, Lokhandi, Bilaspur, Chhattisgarh, India. No collection permit or licence was required for this collection. The collection and use of the plant material complied with applicable local and national guidelines and regulations.

Authors' contributions

Shivshankar Prasad Pandey: synthesis of the $MgFe_2O_4$ nanoparticles, experimental characterization, data analysis, and preparation of the original manuscript. K. P. Tiwari: scientific review, guidance during the study, and interpretation of the results. H. S. Tewari: scientific review, guidance, and interpretation of the results. A. Sharma: assistance with characterization, plotting and presentation of data, data interpretation, and review of the manuscript. V. Sahu: review and critical revision of the manuscript. All authors reviewed and approved the final manuscript.

Ethics, Consent to Participate, and Consent to Publish declarations: not applicable.

References

[1] Ali, S., Khalid, M., Nazir, G., Naz, K., Khan, J. K., Akhtar, M. S., & Abbas, N. (2022). Effect of nickel substitution on structural and dielectric properties of Mg-Zn based spinel ferrite nanoparticles. *Physica Scripta*, *97*(6). https://doi.org/10.1088/1402-4896/AC690F

[2] Almessiere, M. A., Shirsath, S. E., Baykal, A., Mihmanlı, A., Gondal, M. A., & Slimani, Y. (2025). Cation distribution and Electrical/Dielectric features of Ru substituted CoNiCuZn spinel ferrite nanoparticles. *Ceramics International*, *51*(12), 15273–15282. https://doi.org/10.1016/J.CERAMINT.2025.01.363

[3] Araújo, J. C. R., Araujo-Barbosa, S., Souza, A. L. R., Iglesias, C. A. M., Xavier, J., Souza, P. B., Plá Cid, C. C., Azevedo, S., da Silva, R. B., Correa, M. A., de Medeiros, S. N., Silva, E. F., & Bohn, F. (2021). Tuning structural, magnetic, electrical, and dielectric properties of MgFe2O4 synthesized by sol-gel followed by heat treatment. *Journal of Physics and Chemistry of Solids*, *154*. https://doi.org/10.1016/J.JPCS.2021.110051

[4] Chaudhari, H. N., Dhruv, P. N., Meena, S. S., Kavita, S., Basak, C. B., Patni, N., Chauhan, C., &Jotania, R. B. (2026). Effect of annealing temperature on structural, microstructural, and Mössbauer properties of MgFe2O4 ferrite for photo anode application. *Journal of Sol-Gel Science and Technology 2026 117:3*, *117*(3), 77-. https://doi.org/10.1007/S10971-025-07047-2

[5] Desai, H. B., Kumar, A., & Tanna, A. R. (2021). STRUCTURAL and MAGNETIC PROPERTIES of MgFe2O4 FERRITE NANOPARTICLES SYNTHESIS through AUTO COMBUSTION TECHNIQUE. *European Chemical Bulletin*, *10*(3), 186–190. https://doi.org/10.17628/ecb.2021.10.186-190

[6] Dippong, T., Levei, E. A., & Cadar, O. (2021). Recent Advances in Synthesis and Applications of MFe2O4 (M = Co, Cu, Mn, Ni, Zn) Nanoparticles. *Nanomaterials*, *11*(6), 1560. https://doi.org/10.3390/nano11061560

[7] El-Ghazzawy, E. H., Zakaly, H. M. H., Alrowaily, A. W., Saafan, S. A., Ene, A., Abo-aita, N. M., Darwish, M. A., Zhou, D., &Atlam, A. S. (2023). Delving into the properties of nanostructured Mg ferrite and PEG composites: A comparative study on structure, electrical conductivity, and dielectric relaxation. *Heliyon*, *9*(9). https://doi.org/10.1016/j.heliyon.2023.e19745

[8] Fakhry, F., Shaheen, E., El-Dosoky, H., Meaz, T. M., Mubark, M., & El-Shater, R. (2024). Elastic and magnetic characteristics of nano-spinel ferrite Co0.5

MgxCu0.5−xFe2O4. *Scientific Reports*, *14*(1), 29407. https://doi.org/10.1038/S41598-024-74484-4

[9] Gneber, M. Y., Elhamdi, I., Messoudi, J., Dhahri, R., Sahnoune, F., Jemmali, M., Hussein, M., Dhahri, E., & Faria Oliveira Costa, B. (2024). Investigation of variable range hopping and dielectric relaxation in GdCrO3 orthochromite perovskites. *RSC Advances*, *14*(49), 36161–36172. https://doi.org/10.1039/d4ra06104g

[10] Hamdaoui, N., Azizian-Kalandaragh, Y., Khlifi, M., & Beji, L. (2019). Structural, magnetic and dielectric properties of Ni0.6Mg0.4Fe2O4 ferromagnetic ferrite prepared by sol gel method. *Ceramics International*, *45*(13), 16458–16465. https://doi.org/10.1016/J.CERAMINT.2019.05.177

[11] Kefeni, K. K., Msagati, T. A. M., & Mamba, B. B. (2017). Ferrite nanoparticles: Synthesis, characterisation and applications in electronic device. *Materials Science and Engineering: B*, *215*, 37–55. https://doi.org/10.1016/J.MSEB.2016.11.002

[12] Köferstein, R., Walther, T., Hesse, D., & Ebbinghaus, S. G. (2013). Preparation and characterization of nanosized magnesium ferrite powders by a starch-gel process and corresponding ceramics. *Journal of Materials Science*, *48*(19), 6509–6518. https://doi.org/10.1007/s10853-013-7447-x

[13] Kumar, S., & Sreenivas, K. (2024). Influence of sintering temperature on structural, electrical, dielectric, and magnetic properties of magnesium ferrite (MgFe2O4) ceramics prepared using powder derived via Sol-Gel auto-combustion. *Journal of Sol-Gel Science and Technology*, *111*(2), 603–617. https://doi.org/10.1007/S10971-024-06472-Z

[14] Liaskovska, M., Tatarchuk, T., Bououdina, M., & Mironyuk, I. (2019). *Green Synthesis of Magnetic Spinel Nanoparticles* (pp. 389–398). https://doi.org/10.1007/978-3-030-17755-3_25

[15] Pradeep, A., Priyadharsini, P., & Chandrasekaran, G. (2008). Sol–gel route of synthesis of nanoparticles of MgFe2O4 and XRD, FTIR and VSM study. *Journal of Magnetism and Magnetic Materials*, *320*(21), 2774–2779. https://doi.org/10.1016/J.JMMM.2008.06.012

[16] Rashid, A., & Ikram, M. (2025). Dielectric behavior, Complex modulus, and conduction mechanism studies of Ni-doped La2SrFe2-xNixTiO9 triple perovskite for high-frequency electronic applications. *Materials Science and Engineering: B*, *319*. https://doi.org/10.1016/J.MSEB.2025.118332

[17] Revathi, R., Sukumar, M., Kumar, A., Gupta, M., Udhaya, P. A., Sehgal, S. S., Pandit, B., Sundararajan, M., Subramani, A., Dash, C. S., Senthilkumar, N., & Ubaidullah, M. (2024). Facile Synthesis of Ni2+ Doped MgFe2O4 Spinel Nanoparticles: Structural, Optical, Magnetic, and Dielectric Behavior. *Journal of Inorganic and Organometallic Polymers and Materials*, *34*(1), 374–386. https://doi.org/10.1007/S10904-023-02820-8

[18] Salih, S. J., & Mahmood, W. M. (2023). Review on magnetic spinel ferrite (MFe2O4) nanoparticles: From synthesis to application. *Heliyon*, *9*(6), e16601. https://doi.org/10.1016/j.heliyon.2023.e16601

[19] Sharma, A., & Singh, J. (2025). *Green Synthesis of Mgfe2o4 Nanoparticles Using Mangifera Indica Leaf Extract: Investigation of Structural, Optical, Magnetic, and Cytotoxic Properties*. https://doi.org/10.2139/SSRN.5289369

[20] Sharma, R., Thakur, P., Kumar, M., Barman, P. B., Sharma, P., & Sharma, V. (2017). Enhancement in A-B super-exchange interaction with Mn2+ substitution in Mg-Zn ferrites as a heating source in hyperthermia applications. *Ceramics International*, *43*(16), 13661–13669. https://doi.org/10.1016/j.ceramint.2017.07.076

[21] Suresh Kumar, G., Srinivasan, R., Karunakaran, G., Kolesnikov, E., Kim, M., & Karpenkov, D. Y. (2021). Microwave-assisted combustion synthesis of soft ferromagnetic spinel MFe2O4 (M = Ni, Mg, Zn) nanoparticles using Citrus limon fruit extract as a fuel. *Applied Physics A 2021 127:7*, *127*(7), 546-. https://doi.org/10.1007/S00339-021-04694-4

[22] Tahir, M., Imran, M., H Shah, Z., Bilal Riaz, M., Riaz, S., & Naseem, S. (2024). Phase formation and dielectric properties of MgFe2O4 nanoparticles synthesized by hydrothermal technique. *Heliyon*, *10*(8). https://doi.org/10.1016/j.heliyon.2024.e29553

[23] Tank, D., Bharadva, V., Jotania, R. B., Devashrayee, N. M., Chauhan, C. C., & Gor, A. A. (2026). Green synthesis of NiFe2O4 octahedrons using neem extract: magnetic, dielectric, and resistive switching in RF-sputtered film. *Journal of Materials Science: Materials in Electronics 2026 37:8*, *37*(8), 569-. https://doi.org/10.1007/S10854-026-16866-0

[24] Tariq, A., Ullah, U., Ahmad, I., Asif, M., Sadiq, I., & Haleem, H. (2019). Comparative analysis of the Magnesium Ferrite (MgFe2O4) nanoparticles synthesised by three different routes. *IET Nanobiotechnology*, *13*(7), 697–702. https://doi.org/10.1049/iet-nbt.2018.5032

[25] Yu, S. H., Wang, Q. L., Chen, Y., Wang, Y., & Wang, J. H. (2020). Microwave-assisted synthesis of spinel ferrite nanospherolites. *Materials Letters*, *278*. https://doi.org/10.1016/J.MATLET.2020.128431